PHYSICAL REVIEW C **66**, 011304(R) (2002)

Deviations from axial symmetry in ^{181}Os

Zs. Podolyák,[1] S. Al-Garni,[1] R.F. Casten,[2] J.R Cooper,[2,*] D.M. Cullen,[3] A. Dewald,[4] R. Krücken,[2] H. Newman,[1,2] J.N. Orce,[5] C.J. Pearson,[1] C. Ur,[6,†] R. Venturelli,[6] S. Vincent,[1] C. Wheldon,[7,‡] P.M. Walker,[1] F.R. Xu,[1,§] A. Yamamoto,[1] and N.V. Zamfir[2,8,†]

[1]*Department of Physics, University of Surrey, Guildford GU2 7XH, United Kingdom*
[2]*A.W. Wright Nuclear Structure Laboratory, Department of Physics, Yale University, New Haven, Connecticut 06520*
[3]*Department of Physics and Astronomy, University of Manchester, Manchester M13 9PL, United Kingdom*
[4]*Institut für Kernphysik, Univesität zu Köln, Zülpicher Strasse 77, 50937 Köln, Germany*
[5]*School of Engineering, University of Brighton, Brighton BN2 4GJ, United Kingdom*
[6]*Dipartimento di Fisica and INFN, Sezione di Padova, Padova, Italy*
[7]*Department of Physics, University of Liverpool, Liverpool L69 7ZE, United Kingdom*
[8]*Clark University, Worchester, Massachusetts 01610*

(Received 10 May 2002; published 31 July 2002)

Lifetimes of rotational states built on the $7/2^-[514]$ and $1/2^-[521]$ Nilsson single-particle orbitals in ^{181}Os have been measured using the coincidence recoil-distance method. The experimentally determined quadrupole moment, assuming axial symmetry, is $\approx$20% larger for the $7/2^-[514]$ band compared with the $1/2^-[521]$ band. The difference can be understood as an effect of triaxiality. Total Routhian surface calculations show deviations from axial symmetry for both bands, leading to good agreement between theory and experiment.

DOI: 10.1103/PhysRevC.66.011304 PACS number(s): 21.10.Ky, 21.10.Tg, 21.10.Re, 27.70.+q

A variety of shapes may be found for nuclear excited states, although it is difficult to probe deviations from axial symmetry. Multiple Coulomb excitation is a particularly well adapted technique to investigate nuclear shapes [1]. It has been shown, for example, that the ^{186,188,190,192}Os, and ^{194,196}Pt nuclei are β-stiff and γ-soft [2], with decreasing quadrupole collectivity and increasing γ softness (and triaxiality) as the neutron number increases and the $N=126$ closed shell is approached [3,4]. For all these nuclei the effective γ deformation is large, between 15° and 35°.

There is, however, little known about the role of triaxiality in well deformed nuclei. Generally, these nuclei are considered to be axially symmetric, involving triaxiality only for the explanation of a few phenomena. For example, in the Hf-W-Os nuclei with $100 \leqslant N \leqslant 106$, the breakdown of the K selection rule (where K is the projection of the angular momentum on the symmetry axis) leads to relatively short lifetimes of K isomers. This has been explained by quantum tunneling through the γ degree of freedom [5,6], though the possible role of static (equilibrium) γ deformation [7] requires further clarification.

To understand better the role of triaxiality in well deformed nuclei it is a natural choice to study the neutron-deficient osmium isotopes. However, the Coulomb excitation technique is no longer available (the targets would be radioactive) and an alternative approach is required. A sensitive method, used in the present work, is to compare the quadrupole moments of two bands of the same nucleus. Different quadrupole moments could indicate different degrees of triaxiality, assuming that the quadrupole β_2 deformations are similar. In odd-mass nuclei, the γ rigidity can sometimes increase due to the properties of the odd nucleon [8]. Moreover, different single-particle orbitals have different triaxiality-driving effects. Considering the chain of the osmium isotopes, the even-even ^{180,182,184}Os nuclei are the most deformed and most rigid, with the lowest lying first excited (rotational) states, the highest quadrupole transition strengths, and the highest γ-vibrational bandheads $B(E2;2^+ \rightarrow 0^+)$ [9,10]. Therefore, ^{181}Os is a good example to investigate the effect of triaxiality in a well deformed nucleus. Here we present the results of a recent lifetime measurement, using the coincidence recoil-distance (plunger) method [11,12].

The ^{181}Os nucleus has been populated via the ^{160}Gd(^{26}Mg,5n) reaction. The beam was delivered by the tandem accelerator of A.W. Wright Nuclear Structure Laboratory of Yale University. The target consisted of 0.49 mg/cm^2 ^{160}Gd on a 1.5 mg/cm^2 ^{nat}Ta support. It was mounted with the tantalum support facing the beam in the New Yale Plunger Device [13,14] in front of a 6 mg/cm^2 stretched gold stopper foil. The incident beam energy of 124 MeV corresponded to 117 MeV in the middle of the ^{160}Gd target. Data were taken at 15 stopper-target distances between 8 μm and 600 μm. Each flight distance up to 300 μm was controlled and regulated via a piezoelectric feedback system. The γ rays were detected with the SPEEDY Ge-detector array [15], consisting of seven clover detectors plus one $\approx$70% efficient coaxial detector. Events with at least two Ge detectors firing in coincidence were written to tape.

The Ge detectors of the SPEEDY array were organized into three rings at mean angles of 0°, 41.5°, and 138.5° relative

*Present address: Lawrence Livermore National Laboratory, Livermore, CA.
†Permanent address: Institute of Physics and Nuclear Engineering, Bucharest, Romania.
‡Present address: Department of Physics, University of Surrey, Guildford GU2 7XH, UK.
§Permanent address: Department of Technical Physics, Peking University, Beijing 100871, China.

TABLE I. Lifetimes and extracted quadrupole transition strengths in the $1/2^-[521]$ and $7/2^-[514]$ bands of ^{181}Os. The sixth column shows the extracted quadrupole moment assuming axial symmetry. The last column gives the degree of triaxiality according to the potential energy surface calculations. The seventh column shows the quadrupole moment extracted, assuming the theoretical γ deformation.

Band	I^π ($\hbar$)	E_x [17,20] (keV)	τ (ps)	$B(E2;I\rightarrow I-2)$ (e^2 b^2)	Q_0 with $\gamma=0°$ (e b)	Q (e b)	γ (deg)
$1/2^-[521]$	$13/2^-$	677	15.18(106)	1.06(8)	5.83(21)	6.17(22)	+5
	$17/2^-$	1099	5.07(57)	1.16(13)	5.96(34)	6.30(36)	+5
	$21/2^-$	1554	4.05(70)	1.00(17)	5.46(47)	5.77(49)	+5
$7/2^-[514]$	$13/2^-$	491	32.37(158)	0.63(3)	6.78(17)	6.52(16)	−2
	$15/2^-$	682	13.55(82)	0.81(5)	6.66(20)	6.45(20)	−2
	$17/2^-$	891	7.01(54)	1.06(8)	7.02(27)	6.82(26)	−2
	$19/2^-$	1117	3.43(25)	1.34(10)	7.45(27)	7.26(27)	−2
	$21/2^-$	1355	3.34(23)	1.05(7)	6.36(22)	6.20(21)	−2

to the beam axis. For each target-stopper distance the Compton-suppressed $\gamma\gamma$ doubles and higher-fold events were sorted into asymmetric $\gamma\gamma$ matrices with one particular ring on each axis. The three rings correspond to eight different matrices (at 0° there was only one detector), resulting in a total of 120 matrices for the 15 target-stopper distances.

In the analysis of the decay function, the differential decay curve method (DDCM) [11,12] was used. This allows determination of the lifetime of the state of interest unambiguously since the uncertainties about feeding times and intensities are avoided. In the DDCM, one gates on the shifted component of the feeding transition and analyses the stopped (unshifted) and shifted parts of the depopulating transition. The lifetime of the state is given by

$$\tau = \frac{I_u^d}{dI_s^d/dt}, \tag{1}$$

where I_u^d and I_s^d are the intensities of the unshifted and shifted components of the depopulating transition, and $t = d/v$ is the flight time.

In general, the given lifetimes were determined from the sum spectra obtained by gating on all the eight matrices for any target-stopper distance, reducing in this way the statistical errors. These lifetimes were checked by comparing with those obtained from individual matrices, in order to avoid systematic errors. In some cases, depending on the contaminating transitions, some of the matrices were not used.

The velocity of the recoiling nucleus was determined by using the position of the stopped and Doppler-shifted components of the strong transitions in ^{181,182}Os. The obtained recoil velocity of $v = 3.744(30)$ μm/ps corresponds to 1.248(10)% of the speed of light.

The measured lifetimes for the states below the backbending in the bands based on the $1/2^-[521]$ and $7/2^-[514]$ Nilsson orbitals, together with the extracted reduced quadrupole transition probabilities $B(E2)$, are given in Table I. The higher lying levels affected by band crossings will be discussed in a future publication. Examples of lifetime data are given in Fig. 1.

The accurate branching ratios needed to extract the $B(E2)$ values in the $7/2^-[514]$ band (the $1/2^-[521]$ band consists only of $I\rightarrow I-2$ quadrupole transitions in this spin region) were obtained from a high-statistics experiment performed with the Gammasphere Ge array in Berkeley, using the ^{36}S+^{150}Nd reaction [16]. (We note that the branching ratios of previous measurements [17] would lead to the same conclusions.) The dipole-quadrupole mixing of the $I\rightarrow I-1$ transitions and its effect on the internal conversion coefficients were taken into account. The $\delta^2 = I_\gamma(E2;I\rightarrow I-1)/I_\gamma(M1;I\rightarrow I-1)$ mixing-ratio parameter was calculated using the relation $B(E2;I\rightarrow I-2)/B(E2;I\rightarrow I-1) = [\langle IK20|(I-2)K\rangle/\langle IK20|(I-1)K\rangle]^2$, derived from the assumption that the quadruple moment has the same value when extracted both from $B(E2;I\rightarrow I-2)$ and $B(E2;I\rightarrow I-1)$ transition strengths. For the cases presented in this paper the dipole-quadrupole mixing has little effect on the obtained transition strengths due to low internal-conversion coefficients and/or small differences between the $M1$ and $E2$ conversion coefficients, and the uncertainties caused by the mixing are within the given error limits.

Assuming that the K structure of the wave functions does not change significantly with spin, the intrinsic quadrupole moment can be obtained from the intraband transition strengths using the formula [18]

$$Q^2 = \frac{8\pi}{5} B(E2;I\rightarrow I-2)\frac{(2I-1)(2I+1)}{(I-1)I}\left[\cos(\gamma+30°) - \cos(\gamma-30°)\frac{K^2}{(I-1)I}\right]^{-2}. \tag{2}$$

We note that in the majority of previous works only axial deformation is considered, for which the quadrupole moment comes from the expression $Q_0^2 = (16\pi/5)B(E2;I\rightarrow I-2)/\langle IK20|I-2K\rangle^2$. In this paper we generally use the notation Q for the intrinsic quadrupole moment, and Q_0 is used only for the special case when $\gamma=0°$ is considered. In Eq. (2) the sign of the γ value specifies the orientation relative to the rotation axis according to the Lund convention [19].

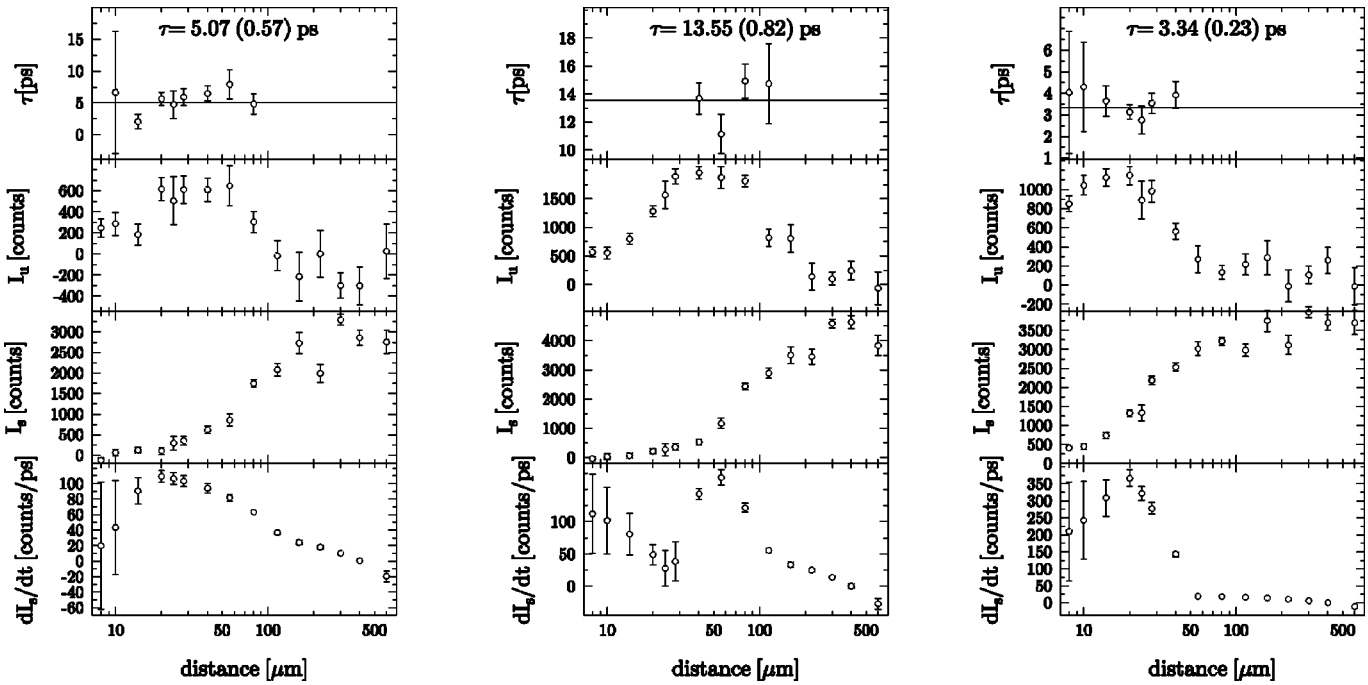

FIG. 1. Examples of lifetime analysis for the $17/2^-$ state of the $1/2^-[521]$ band, and $15/2^-$ and $21/2^-$ levels of the $7/2^-[514]$ band, respectively. For each distance, the value of the mean life (upper panel) is deduced from the intensity of the unshifted component I_u (second panel from the top) and from the corresponding time derivative dI_s/dt of the shifted component (lower panel) of the depopulating transition. The intensity of the unshifted component is also shown (second panel from the bottom).

The quadrupole moments calculated assuming axial symmetry ($\gamma=0°$) are given in Table I. With the assumption of $\gamma=0°$, the quadrupole moment within the $K=7/2$ band is found to be 17% higher than that in the $K=1/2$ band. The weighted average quadrupole moments Q_0 are $6.79(10)e$ b and $5.81\ (17)e$ b, respectively, leading to a difference of $0.98(19)e$ b. This would correspond to 16% difference in quadrupole deformation β_2. Since the quadrupole moments in the two bands were extracted from the same experiment using the same procedure, the difference of the Q_0 values is largely free of systematic errors. Although a possible reason for the different quadrupole moments in the two bands could be a change in the magnitude of the quadrupole deformation β_2, a more probable origin is connected with triaxiality.

To get a deeper understanding of the nuclear shape, total routhian surface (TRS) calculations were performed. The nonaxial deformed Woods-Saxon potential [21] is employed. Collective rotation is investigated in the frame of the cranked shell model in the three-dimensional deformation spaces of β_2, γ, and β_4. Both monopole and double-stretched quadrupole pairings are included [22]. The monopole pairing strength G is determined by the average-gap method [23], and quadrupole pairing strengths are obtained by restoring the Galilean invariance broken by the seniority pairing force [24]. To avoid the spurious phase transition encountered in the BCS approach, we use approximate particle-number projection by means of the Lipkin-Nogami method [25]. Pairing correlations are dependent on the rotational frequency and deformation. In order to include such dependence in the TRS, we have performed pairing-deformation-frequency self-consistent TRS calculations, i.e., for any given deformation and frequency, pairings are self-consistently calculated by the HFB-like method [25]. At a given frequency, the deformation of a state is determined by minimizing the calculated TRS.

The calculations indicate no significant shape changes below the backbending, and typical TRS plots corresponding to the two bands of interest are shown in Fig. 2. According to the calculations, the $K=1/2$ states are slightly *more* quadrupole deformed than the $K=7/2$ states (contrary to the naive

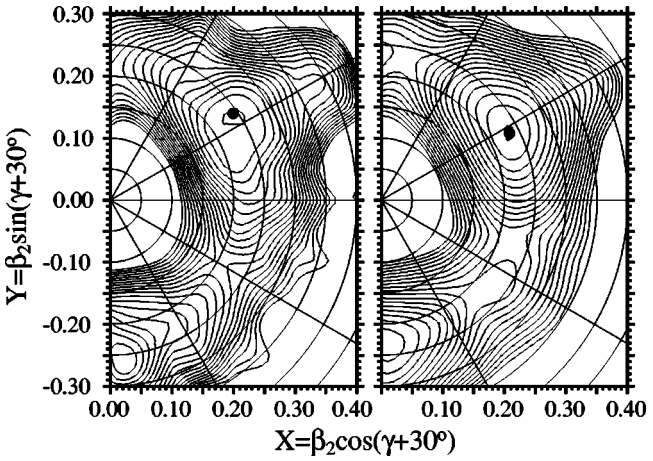

FIG. 2. Total Routhian surface calculations for the $1/2^-[521]$ (left panel) and $7/2^-[514]$ (right panel) configurations of ^{181}Os at a rotational frequency $\hbar\omega=0.1$ MeV, corresponding to spin $I \approx 5-6$. The energy difference between two successive contour lines is 200 keV. The two minima are at $\beta_2=0.243$, $\beta_4=-0.031$, $\gamma=+5°$ and $\beta_2=0.234$, $\beta_4=-0.033$, $\gamma=-2°$, respectively.

interpretation given above), with a value of $\beta_2 = 0.243$ compared to $\beta_2 = 0.234$. However, the TRS calculations give not only a stable β_2 deformation, but also a deviation from axial symmetry with $\gamma = +5°$ and $\gamma = -2°$, respectively. Using these γ deformations, the experimental quadrupole moments were reevaluated according to Eq. (2), and they are given in the seventh column of Table I. Positive γ increases the quadrupole moment, while negative γ decreases it. (We note that the calculations give also a hexadecapole deformation of $\beta_4 = 0.03$ for both bands. The obtained β_2 and β_4 values fit very well into the systematics of the region [26,27].)

The theoretical intrinsic quadrupole moment was extracted as $Q = \Sigma 2 V_k^2 q_k$, where q_k are the single-proton quadrupole moments obtained from the Woods-Saxon wave functions and V_k^2 are the occupation probabilities. The quadrupole moment Q has contributions from two spherical-tensor components, $Q = Q_{20} + Q_{22}$. The Q_{20} term depends on the β_2 quadrupole deformation and it is independent of the degree of triaxiality. The Q_{22} term vanishes for axially symmetric nuclei, being negative for positive γ and positive for negative γ deformations.

The theoretical and experimental quadrupole moments are compared in Fig. 3. In the $K = 1/2$ band the theoretical quadrupole moment is almost constant, $Q = 6.2$ e b, without significant spin dependence. The experimental values extracted considering $\gamma = 0°$ are considerably lower for all three states. However, when the theoretically predicted $\gamma = +5°$ is used, the Q values extracted from the lifetimes agree very well with the theory.

In the case of the $K = 7/2$ band, the predicted γ deformation, $\gamma = -2°$, is smaller (and with opposite sign) than for the $K = 1/2$ band. Therefore, it has a smaller effect on the quadrupole moment. The quadrupole moment extracted assuming axial symmetry is slightly larger than the calculated quadrupole moment $Q = Q_{20} + Q_{22}$ with $\gamma = -2°$, and on average 0.4 eb higher than the Q_{20} term. Adopting the theoretical γ deformation, the Q values extracted from the experiment again agree with the theory. As seen in Fig. 3, both the experimental and theoretical quadrupole moments increase slightly with spin. (We note that the drop in the measured Q value at spin $I = 21/2$ might be the effect of the backbending, where there is a reduced overlap of the wave functions of the initial and final states involved.)

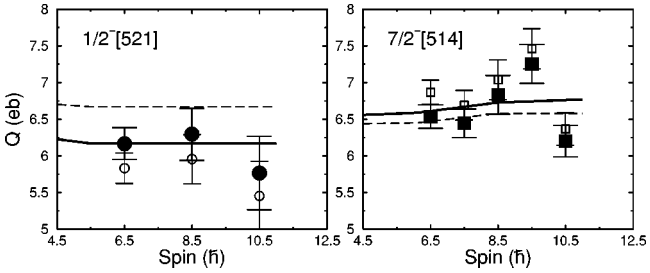

FIG. 3. Quadrupole moments as function of spin for the $1/2^-[521]$ (left panel) and $7/2^-[514]$ (right panel) bands, respectively. The filled symbols indicate the experimental quadrupole moments, assuming the γ deformation predicted by the theoretical calculations, $+5°$ for the $1/2^-[521]$ band, and $-2°$ for the $7/2^-[514]$ band, respectively. The open symbols indicate the values assuming $\gamma = 0$. The solid lines show the theoretical $Q = Q_{20} + Q_{22}$ value. The dotted lines show the theoretical quadrupole moments without triaxiality (Q_{20}).

We conclude that agreement between theory and experiment could only reasonably be obtained by employing deviations from axial symmetry. An overall adjustment of β_2 cannot give such a good agreement. The presence of two bands with opposite γ signs in the same nucleus shows the sensitivity to axial asymmetry. The present experiment illustrates that even a small γ deformation can have a measurable effect on the quadrupole moment and this needs to be taken into account if a quantitative understanding of $E2$ transition rates is to be obtained.

The authors thank the staff of the tandem accelerator for providing a high quality beam. The authors are grateful to R. Wyss and P. H. Regan for useful discussions. This work was supported in part by EPSRC (U.K.) and by the U.S. DOE Grant Nos. DE-FG02-91ER-40609 and DE-FG02-88ER-40417.

[1] K. Kumar, Phys. Rev. Lett. **28**, 249 (1972).
[2] R.F. Casten and J.A. Cizewski, Nucl. Phys. **A309**, 477 (1978).
[3] C.Y. Wu *et al.*, Nucl. Phys. **A607**, 178 (1996).
[4] A. Mauthofer *et al.*, Z. Phys. A **336**, 263 (1990).
[5] T. Bengtsson *et al.*, Phys. Rev. Lett. **62**, 2448 (1989).
[6] K. Narimatsu, Y.R. Shizuma, and T. Shizuma, Nucl. Phys. **A601**, 69 (1996).
[7] F.R. Xu, P.M. Walker, J.A. Sheikh, and R. Wyss, Phys. Lett. B **435**, 257 (1998).
[8] A. Granderath *et al.*, Nucl. Phys. **A597**, 427 (1996).
[9] S. Raman, C.W. Nestor, and P. Tikkanen, At. Data Nucl. Data Tables **78**, 1 (2001).
[10] R. F. Firestone *et al.*, *Table of Isotopes*, 8th ed. (Wiley, New York, 1996).
[11] A. Dewald, S. Harissopulos, and P. von Brentano, Z. Phys. A **334**, 163 (1989).
[12] G. Böhm, A. Dewald, P. Petkov, and P. von Brentano, Nucl. Instrum. Methods Phys. Res. A **329**, 248 (1993).
[13] R. Krücken, J. Res. Natl. Inst. Stand. Technol. **105**, 53 (2000).
[14] A. Dewald *et al.*, Nucl. Phys. **A545**, 822 (1992).
[15] R. Krücken, *Applications of Accelerators in Research and Industry* (*CAARI 2000*) (AIP, New York, in press).
[16] D. M. Cullen *et al.*, (unpublished).
[17] T. Kutsarova *et al.*, Nucl. Phys. **A587**, 111 (1995).
[18] P. Petkov *et al.*, Nucl. Phys. **A640**, 293 (1998).
[19] G. Andersson *et al.*, Nucl. Phys. **A268**, 205 (1976).
[20] R.B. Firestone, Nucl. Data Sheets **62**, 101 (1991).
[21] W. Nazarewicz, J. Dudek, R. Bengtsson, T. Bengtsson, and I. Ragnarsson, Nucl. Phys. **A435**, 397 (1985).
[22] W. Satuła and R. Wyss, Phys. Rev. C **50**, 2888 (1994); W. Satuła and R. Wyss, Phys. Scr. **T56**, 159 (1995).

[23] P. Möller and J.R. Nix, Nucl. Phys. **A536**, 20 (1992).
[24] H. Sakamoto and T. Kishimoto, Phys. Lett. B **245**, 321 (1990).
[25] W. Satuła, R. Wyss, and P. Magierski, Nucl. Phys. **A578**, 45 (1994).
[26] R. Bengtsson, S. Frauendorf, F.-R. May, and At. Data At. Data Nucl. Data Tables **35**, 15 (1986).
[27] W. Nazarewicz, M.A. Riley, and J.D. Garrett, Nucl. Phys. **A512**, 61 (1990).